ACS APPLIED MATERIALS & INTERFACES

Research Article

www.acsami.org

Diffusion of Ag into Organic Semiconducting Materials: A Combined Analytical Study Using Transmission Electron Microscopy and X-ray Reflectivity

Stefanie Fladischer,*[†] Alfred Neuhold,[‡] Elke Kraker,[§] Thomas Haber,[†] Bernhard Lamprecht,[§] Ingo Salzmann,[⊥] Roland Resel,[‡] and Werner Grogger[†]

[†]Institute for Electron Microscopy and Fine Structure Research, Graz University of Technology & Graz Centre for Electron Microscopy, Graz, Austria

[‡]Institute of Solid State Physics, Graz University of Technology, Graz, Austria

[§]Institute for Surface Technologies and Photonics, Joanneum Research Forschungsgesellschaft mbH, Weiz, Austria

[⊥]Department of Physics, Humboldt-Universität zu Berlin, Berlin, Germany

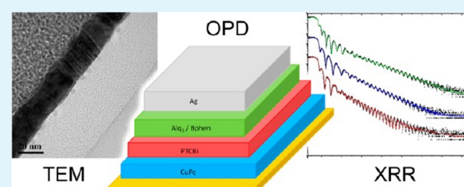

ABSTRACT: This study shows that the morphology of organic/metal interfaces strongly depends on process parameters and the involved materials. The interface between organic n-type blocking layer materials and the top Ag cathode within an organic photodiode was investigated. Ag was deposited on either amorphous tris-8-hydroxyquinolinato-aluminum (Alq_3) or crystalline 4,7-diphenyl-1,10-phenanthroline (Bphen) using different deposition techniques such as electron beam deposition, ion beam sputtering, and vacuum thermal evaporation at various deposition rates. The interfaces were studied by transmission electron microscopy and X-ray reflectivity. It was found that Bphen does not show any Ag diffusion no matter which deposition technique was used, whereas the Ag diffusion into Alq_3 depends on the deposition technique and the deposition rate. The highest amount of Ag diffusion into Alq_3 occurred by using thermal vacuum deposition at low deposition rates.

KEYWORDS: *Ag diffusion, Alq_3, Bphen, organic/metal interface, TEM, XRR*

INTRODUCTION

The performance and efficiency of organic electronic devices depend on several aspects, such as intrinsic material properties and the interfaces between the different materials. Especially, the roughness of organic/metal interfaces and material diffusion distinctly influence the device performance. Furthermore, the influence of organic blocking layers introduced into device structures in combination with different deposition techniques of metal electrodes, e.g., Ag, are of particular importance.

For our present study on organic/metal interfaces an organic photodiode (OPD), which is used as detection unit in a sensor platform, was chosen as test device.[1−3] The setup of this OPD is based on the well-known Tang[4] photodiode, consisting of stacked layers of copper phthalocyanine (CuPc as p-type material) and perylene tetracarboxylic bisbenzimidazole (PTCBi as n-type material). A thin Au layer was used as semitransparent bottom electrode and an opaque Ag layer was deposited as top electrode. Tris-8-hydroxyquinolinato-aluminum (Alq_3, n-type material) and 4,7-diphenyl-1,10-phenanthroline (Bphen, n-type material) were introduced as additional layer between the organic stack and the cathode as such blocking layers are reported to improve the device performance.[5,6] The chemical structures of the respective molecules and the layout of the OPDs are depicted in Figure 1 together with a transmission electron microscopy (TEM) image of the cross-section of a representative OPD with Bphen as a blocking layer.

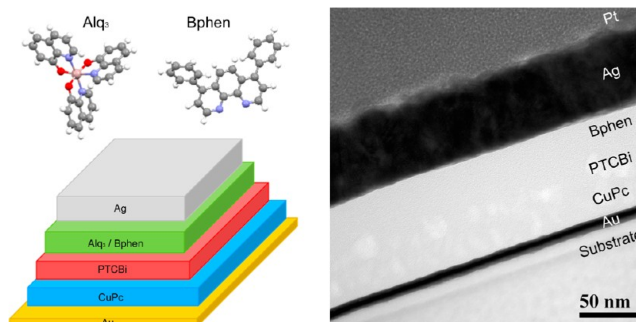

Figure 1. Chemical structure of tris-8-hydroxyquinolinato-aluminum (Alq_3) and 4,7-diphenyl-1,10-phenanthroline (Bphen), layout and TEM cross-section image of the organic photodiode (Bphen used as a blocking layer, Ag electrode deposited by vacuum thermal evaporation).

As organic/metal interfaces play an important role for the device performance, numerous studies on metal diffusion into organic layers have been carried out[7−17] within which a variety of experimental techniques have been used including TEM,[8,9,16] X-ray reflectivity,[16,17] X-ray photoelectron spectroscopy,[9,10,12,14]

Received: July 30, 2012
Accepted: October 1, 2012
Published: October 1, 2012

 © 2012 American Chemical Society

secondary ion-mass spectrometry,[11,13] radiotracer measurements,[8,9,15] and Rutherford backscattering.[8,13,16] Although some data on Ag diffusion into Alq_3[10−14] was already reported, to the best of our knowledge, no study was carried out on Ag diffusion into Bphen yet. The above-mentioned studies report conflicting results on Ag diffusion into Alq_3 including clear evidence that diffusion does occur[10,11] and the presence of well-defined interfaces without chemical reactions.[12,13]

In this study, we investigated Ag diffusion into both Alq_3 and Bphen with respect to different Ag deposition techniques such as electron beam deposition (EBD), ion beam sputtering (IBS), and vacuum thermal evaporation (VTE) at various deposition rates. The interfaces were characterized combining transmission electron microscopy (TEM), favored for its high spatial resolution, and X-ray reflectivity (XRR) as bulk characterization tool, as outlined in ref 18. Herewith, the dependence of interfacial parameters such as roughness and material diffusion on the fabrication procedure of the top Ag cathode was investigated. Finally, the findings for the interfaces were related to the device performances.

■ EXPERIMENTAL DETAILS

Materials. For this study we fabricated OPDs and additional test structures comprising Alq_3 or Bphen layers with top Ag layers only. All samples were produced in a high-vacuum clustertool (Oerlikon Leybold Vacuum GmbH) including a metal deposition chamber (EBD, IBS and VTE) and an organic material deposition chamber (4 effusion cells). A transfer chamber connects the metal and the organic deposition chamber without breaking the vacuum during the whole sample fabrication procedure. All evaporated layers were thus prepared under high vacuum conditions (1×10^{-6} mbar) at room temperature by rotating the substrate to ensure homogeneous coating. The film thickness was triggered with a quartz thickness gauge.

For the OPDs, microscope glass slides were used as substrates. For the semitransparent anode, a 6 nm Au layer was deposited by physical sputtering. The organic layer stack was formed by a 30 nm CuPc film (p-type semiconductor, purchased from Fluka), a 30 nm film of PTCBi (n-type semiconductor, purchased from Sensient Imaging Technologies GmbH), and 37 nm Alq_3 or Bphen (blocking layer, both purchased from Sigma Aldrich). As top-electrode an opaque Ag layer of 80 nm was deposited with an area of 9 mm^2, which determines the active device area. Four different deposition techniques were used: electron beam deposition (EBD), ion beam sputtering (IBS), and vacuum thermal evaporation (VTE) with deposition rates of 0.02 and 0.3 nm/s. To provide reproducibility for the current to voltage characteristic measurements, we fabricated every OPD configuration differing in the organic material and/or the Ag deposition technique 6 times.

Samples for studying the interfaces were deposited on silicon wafers with 150 nm thermally oxidized SiO_2 (from Siegert Consulting e.K.). The organic blocking layer materials Alq_3 and Bphen were deposited with a nominal film thickness of 40 nm. For these samples a 20 nm thin Ag layer was chosen enabling accurate XRR measurements. For each organic/Ag configuration two samples, one for TEM and one for XRR investigations, were produced simultaneously to guarantee their equality. Ag deposition using VTE was performed at different deposition rates, 0.02, 0.1, 0.5, and 1 nm/s. The deposition rates for EBD and IBS were 0.03 and 0.7 nm/s, respectively.

Methods. Current to voltage ($I-V$) characteristics of the OPDs were determined using a 150 W EKE halogen lamp. The light was launched into a fibreoptic cable and led to a single backlight, which had an area of 2 in. × 2 in. and was positioned under a glass window. The samples were placed on the glass window and contacted from the top with contact needles. The $I-V$ characteristic was measured using an MB1020 parameter analyzer from mb-technologies. Additionally, the measurement desk was equipped with an opaque shield to block ambient light during the measurements.

For TEM investigations cross-section samples were made using a focused ion beam (FIB) instrument. The in situ lift-out technique[19] was chosen to realize homogeneously thin cross-section lamellas. To protect the surface from beam damage Pt layers were grown in the FIB by electron-beam induced deposition followed by ion-beam assisted deposition. To avoid artificial ion beam induced Ag diffusion into the organic materials upside down milling was used. To prevent Ag from degradation in ambient air, we started TEM investigations immediately after preparing the lamella. For the TEM investigations, an FEI Tecnai F20 (S)TEM with a Schottky field-emission gun (FEG) operated at 200 kV equipped with a high-resolution Gatan Imaging Filter (GIF) and a Sapphire Si(Li) detector for energy dispersive X-ray spectrometry was used. To elucidate the interfaces, we chose TEM bright-field (BF) and high-angle annular dark field (HAADF) imaging techniques.

XRR measurements were performed on a Panalytical Empyrean Reflectometer setup with a 1/32° primary slit (vertical limitation), a 10 mm beam mask (horizontal limitation) and a multilayer mirror on the primary side using Cu−Kα radiation (λ = 0.154 nm). A small receiving slit of 0.1 mm and a PANalytical PIXCEL^{3D} detector were used at the secondary side. The X'Pert Reflectivity 1.3 software package was used to simulate the experimental data, which uses the Parratt formalism.[20] In addition, this software package comprises a genetic fitting algorithm,[21] which finds the vicinity of the global optimum of the fit and uses the Marquardt−Levenberg algorithm to finally optimize the parameters according to the local minimum. The surface roughness and the interface roughness were determined using the Nevot and Croce approach.[22] The results of the XRR measurements are presented using the out-of-plane (q_z) component of the scattering vector $\mathbf{q}$ as the abscissa.

Grazing incidence X-ray diffraction (GIXD) was measured to probe the crystallographic structure of the organic layers. The measurements were performed at the beamline W1 of the synchrotron radiation source HASYLAB (DESY, Hamburg, Germany) using a wavelength of 0.118 nm. The incidence angle of the X-ray beam was set to $\alpha_i = 0.15°$ and the diffracted beam was measured with a one-dimensional MYTHEN II detector. The results are presented as integrated intensities of the reciprocal space map as a function of the in-plane component q_p of the scattering vector $\mathbf{q}$.

■ RESULTS AND DISCUSSION

The OPDs were characterized by $I-V$ measurements to gain insight into the electrical behavior and the performance of the devices, TEM and XRR investigations were performed to structurally characterize the organic/metal interfaces, and GIXD was carried out on the Alq_3 and Bphen blocking layers to determine their crystallographic structure.

Figure 2 depicts linescans extracted from individual reciprocal space maps integrated up to 0.65 Å^{-1} along the out-of-plane component of the scattering vector (q_z) of the pristine SiO_2 substrate (black curve), the Alq_3 layer (red curve), and the Bphen layer (blue curve) as a function of the in-plane component of the scattering vector (q_p). SiO_2 was used as substrate for both organic materials due to its low surface roughness ideal for GIXD. Our data clearly evidence amorphous growth of Alq_3 on the amorphous SiO_2 substrate and, in contrast, crystalline growth of Bphen. The Bphen diffraction peaks were indexed by the unit-cell parameters published recently by Li et al.[23]

The investigated organic photodiodes are employed as detection unit in opto-chemical sensor applications. Such integrated sensor OPDs are used to quantify changes of light corresponding to different kinds of gas concentrations as described in ref 3. Note that a high ON/OFF ratio (ON: photodiode current under illumination, OFF: dark current) of the corresponding OPDs is essential to reach a high resolution

dx.doi.org/10.1021/am301504j | ACS Appl. Mater. Interfaces 2012, 4, 5608−5612

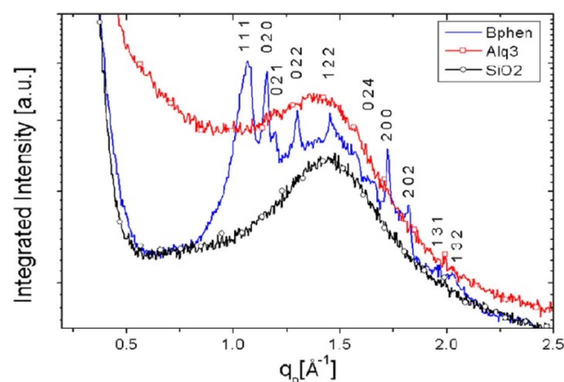

Figure 2. Intensity of the reciprocal space map (integrated along q_z) as a function of the in-plane component of the scattering vector (q_p) from GIXD. Black curve, amorphous SiO_2 substrate; red curve, amorphous Alq_3 layer; blue curve, crystalline Bphen layer with the corresponding Miller indices.

of the sensor. ON/OFF ratios (measured at 0 V) of more than 1×10^3 are necessary for reliable sensor performance.

The *I*−*V* characteristics of the investigated OPDs showed (i), that the two organic blocking layer materials lead to different device performances and, (ii), that the different Ag deposition techniques significantly impact the *I*−*V* characteristics. Figure 3 depicts representative *I*−*V* characteristics in dark and under white light illumination for the OPDs using Bphen as blocking layer.

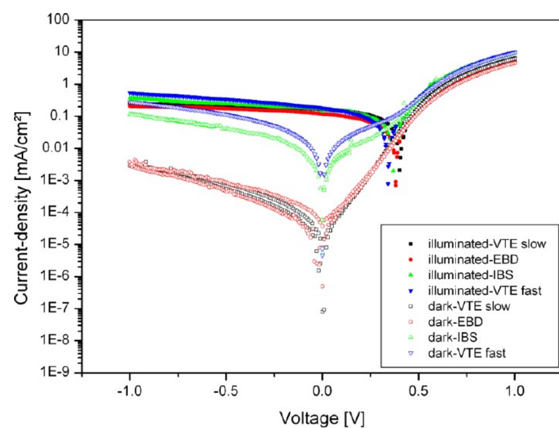

Figure 3. Current−density vs voltage characteristics of organic photodiodes using Bphen as blocking layer under illumination (10 mW/cm^2) and in dark. The Ag electrodes were produced by vacuum thermal evaporation (VTE), electron beam deposition (EBD), and ion beam sputtering (IBS).

OPDs with Ag deposited slowly by VTE (Figure 3, black lines) reached the highest ON/OFF ratios of 1×10^5, followed by EBD (red lines) yielding an ON/OFF ratio of 1×10^4, whereas devices fabricated by IBS (green lines) and fast VTE (blue lines) reached only 1×10^2.

For the TEM characterization of the present organic/metal interfaces BF imaging was performed to get spatially resolved information about the morphology of the different materials and their interfaces. Additionally, HAADF imaging was used to gain contrast between the organic materials and the Ag layer due to the dependence of electron scattering on the atomic number. For each specimen the interfaces were investigated over a range of 5 μm (i.e., width of lamella) and the presented images are representative for the whole lamella.

In Figure 4, TEM cross-section images of the Alq_3/Ag stacks on Si/SiO_2 substrates using different Ag deposition techniques

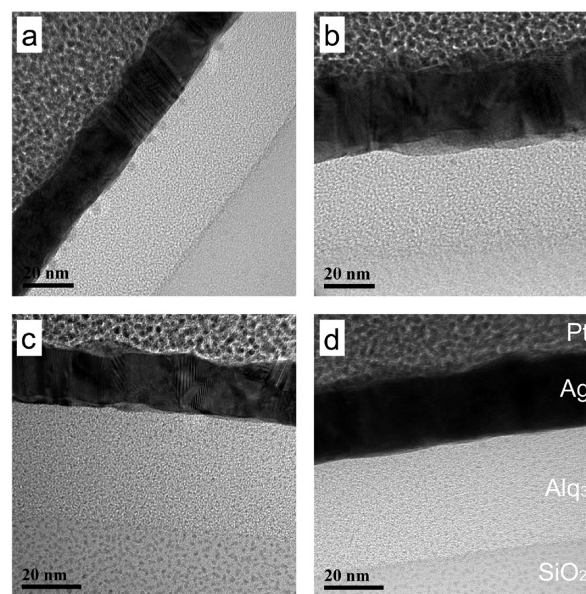

Figure 4. TEM cross-section images of the SiO_2/Alq_3/Ag stack with an additional Pt protection layer. The Ag layers were deposited on Alq_3 by (a) vacuum thermal evaporation with a deposition rate of 0.02 nm/s and (b) 1 nm/s, by (c) electron beam deposition and (d) ion beam sputtering.

are shown. In all images the lowest layer is the SiO_2 substrate followed by Alq_3, Ag and the Pt protection layer. Figure 4a represents a specimen where Ag was deposited by VTE with the lowest investigated deposition rate of 0.02 nm/s. There, Ag diffusion into Alq_3 can clearly be observed by means of small Ag particles at the interface penetrating into the organic layer over a range of approximately 6 nm. Additional EDXS measurements proved these particles to be Ag. Similar Ag diffusion to a smaller extent was detected for the samples where Ag was deposited by VTE with the highest investigated deposition rate of 1 nm/s (Figure 4b). Interestingly, the diffusion depth is essentially identical, whereas the amount of diffused Ag particles is significantly reduced. This clearly indicates that Ag deposition on Alq_3 using VTE induces Ag diffusion into the organic layer. Moreover, depending on the deposition rate Ag diffusion occurs to a varying extent: the lower the deposition rate the more Ag diffuses into Alq_3. Images c and d in Figure 4 display the specimens with Ag top layers deposited by EBD and IBS, respectively. In both cases, no Ag particles penetrating into Alq_3 were observed. Therefore, obviously, Ag diffusion into Alq_3 can be minimized by choosing EBD or IBS as Ag deposition technique.

Figure 5 shows TEM cross-section images of the Bphen/Ag stacks on Si/SiO_2 substrates using different Ag deposition techniques. The images show the same assembly as in Figure 4 for Alq_3 with Bphen instead. Images a and b in Figure 5 depict Ag deposited by VTE at deposition rates of 0.02 and 1 nm/s, respectively. Figure 5c displays Ag deposited by EBD and d shows IBS deposited Ag. In the case of Bphen, no Ag diffusion was observed, regardless of both deposition technique and rate. Furthermore, comparing the interfaces to Ag of the two organic

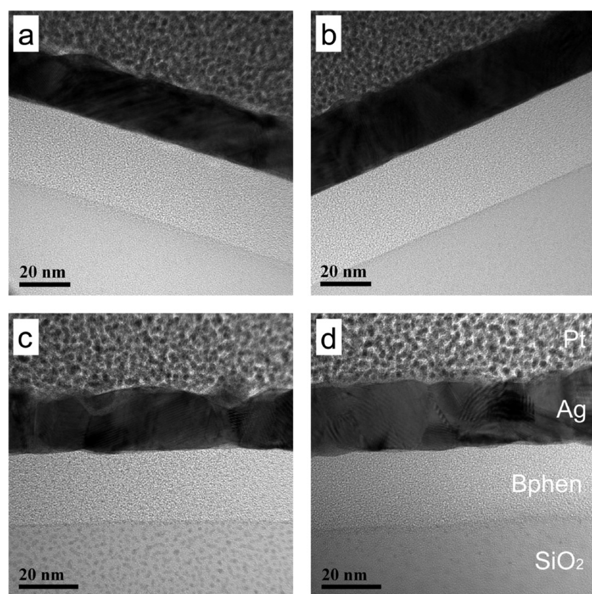

Figure 5. TEM cross-section images of the SiO_2/Bphen/Ag stack with an additional Pt protection layer. The Ag layers were deposited on Bphen by (a) vacuum thermal evaporation with a deposition rate of 0.02 nm/s and (b) 1 nm/s, by (c) electron beam deposition and (d) ion beam sputtering.

materials, it is evident that the interface of Bphen to Ag is significantly more defined than that of Alq_3.

XRR measurements were performed to obtain information on layer thickness, interface roughness and electron density of the respective layers. Figure 6 shows the experimental XRR data (black dots) of the Si/SiO_2/Alq_3/Ag and Si/SiO_2/Bphen/Ag samples for different deposition techniques of the top Ag layer together with the corresponding simulations (lines). Note that in the case of Alq_3 the experimental data were simulated with an additional layer between Alq_3 and Ag to improve the quality of the fit, as without this layer, the minima of the Kiessig fringes could not be reasonably reproduced.[24] The introduction of such an additional layer was already reported by Gautier et al.[17] The parameters of this additional layer depend on the deposition technique as well as the deposition conditions. In Figure 7, the thickness and electron density of this additional layer are depicted. The rather thin additional layers (0.5−2.3 nm) exhibit increased electron densities compared to that of pure Alq_3 (0.42 Å^{-3}). Its thickness in combination with its electron density can be interpreted in terms of diffusion depth and amount of diffused metal. The thickness of the diffusion layer is largest when the deposition rate is lowest, and therefore, decreases with increasing deposition rate, which is fully in-line with our TEM results. For EBD and IBS, where no Ag diffusion could be detected by TEM, the thickness of the additional layer, proposed for the XRR fit, is significantly lower (0.5−1 nm), which is in the range of the interface roughness (0.5 nm). In contrast to the Alq_3 multilayer stack, the simulations for Bphen could be properly performed without any diffusion layers, which points to a well-defined Bphen/Ag interface and no Ag diffusion into the subjacent organic material, which is, again, in good agreement with our TEM results. Note that, in comparison to Alq_3, Bphen possesses a smaller electron density (0.37 Å^{-3}).

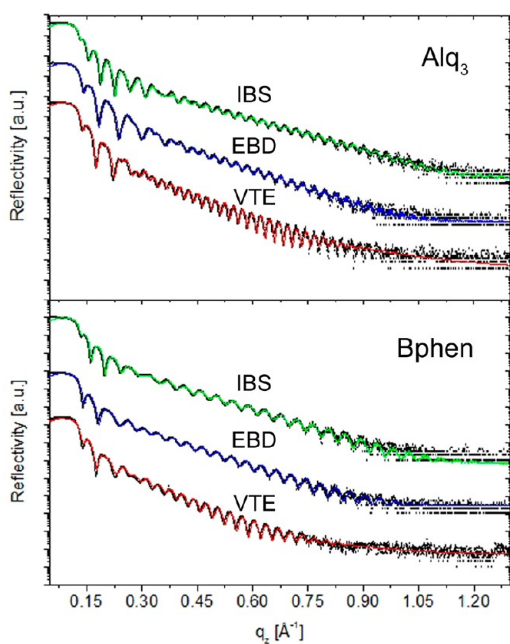

Figure 6. XRR measurements (black dots) and simulated data (full lines) of the Si/SiO_2/Alq_3/Ag and the Si/SiO_2/Bphen/Ag stacks. The figures compare samples with Ag layers deposited by ion beam sputtering (IBS, green line), electron beam deposition (EBD, blue line) and vacuum thermal evaporation (VTE, red line, deposition rate 0.02 nm/s).

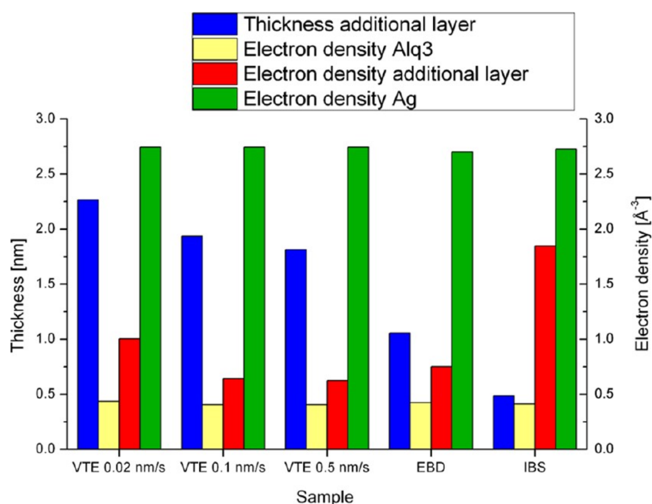

Figure 7. XRR fit results for the additional layer (diffusion layer) introduced between Alq_3 and Ag in the simulation. Its thickness and electron density are depicted together with the electron densities of Alq_3 and Ag for the different samples, where Ag is deposited by vacuum thermal evaporation (VTE) at various deposition rates (0.02, 0.1, 0.5 nm/s), electron beam deposition (EBD), and ion beam sputtering (IBS).

Overall, the results of our TEM and XRR investigations are both qualitatively and quantitatively in good agreement and, hence, corroborate each other. From these results, it becomes clear that Ag diffusion essentially depends on the nature of subjacent organic material. We attribute the different Ag diffusion behavior into the two different organic materials to the degree of order within the organic layers: severe diffusion into amorphous Alq_3 occurs while a well-defined organic/metal interface in case of crystalline Bphen exists. Furthermore, the

deposition technique has a substantial impact on the diffusion behavior and the interface morphology, which all is confirmed by the *I*−*V* characteristics.

CONCLUSIONS

First, this work shows that the combination of TEM and XRR represents a powerful nanoanalytical toolset perfectly suited for the characterization of organic electronic devices. The diffusion behavior of Ag could therewith be elucidated: No Ag diffusion was detected in the case of crystalline Bphen, whereas Ag diffusion of tunable extent was observed for amorphous Alq_3, which depends on both the deposition technique and the deposition rate. Ag deposited on Alq_3 using VTE induces Ag diffusion: the lower the deposition rate the more Ag diffuses into Alq_3. In contrast, no Ag diffusion was detected for Ag deposited by EBD and IBS. The Ag diffusion behavior therefore clearly depends on the crystallinity of the organic materials (amorphous Alq_3 vs crystalline Bphen). Additionally, *I*−*V* characteristics confirm this material and deposition technique dependence. Regarding both the amount of diffused material and its diffusion depth, the process of Ag diffusion entails issues of short-circuits and the transition to ohmic diode characteristics. Clearly, to optimize the device performance, an appropriate deposition parameter set needs to be found for each individual material stack. In the present case for OPDs, the most reliable production strategy consists of using Bphen in combination with Ag deposited by VTE with the lowermost deposition rate.

In summary, we demonstrated that Ag diffusion essentially depends on the structural properties of the subjacent organic material and that diffusion, in turn, can be minimized by choosing appropriate materials, deposition techniques, and preparation parameters. Both the deposition technique used for the metallic layer and the nature of the organic blocking layer material itself significantly impact the performance of organic semiconducting devices.

AUTHOR INFORMATION

Corresponding Author

*Tel.: +43 316 8738831. Fax: +43 316 873108831. E-mail: stefanie.fladischer@felmi-zfe.at.

Notes

The authors declare no competing financial interest.

ACKNOWLEDGMENTS

Financial support by the “Austrian NANO Initiative” (ISOTEC national cooperative RTD project 819718) and the Deutsche Forschungsgemeinschaft (DFG) are kindly acknowledged. We thank W. Caliebe (HASYLAB, DESY) for experimental support.

REFERENCES

(1) Kraker, E.; Haase, A.; Lamprecht, B.; Jakopic, G.; Konrad, C.; Köstler, S. *Appl. Phys. Lett.* **2008**, *92*, 033302.
(2) Lamprecht, B.; Abel, T.; Kraker, E.; Haase, A.; Konrad, C.; Tscherner, M.; Köstler, S.; Ditlbacher, H.; Mayr, T. *Phys. Status Solidi RRL* **2010**, *4*, 157−159.
(3) Lamprecht, B.; Kraker, E.; Sagmeister, M.; Köstler, S.; Galler, N.; Ditlbacher, H.; Ungerböck, B.; Abel, T.; Mayr, T. *Phys. Status Solidi RRL* **2011**, *5*, 344−346.
(4) Tang, C. W. *Appl. Phys. Lett.* **1986**, *48*, 183−185.
(5) Song, Q.; Li, F.; Yang, H.; Wu, H.; Wang, X.; Zhou, W.; Zhao, J.; Ding, X.; Huang, C.; Hou, X. *Chem. Phys. Lett.* **2005**, *416*, 42−46.
(6) Huang, Q.; Walzer, K.; Pfeiffer, M.; Leo, K.; Hofmann, M.; Stübinger, T. *J. Appl. Phys.* **2006**, *100*, 064507.
(7) Hirose, Y.; Kahn, A.; Aristov, V.; Soukiassian, P.; Bulovic, V.; Forrest, S. R. *Phys. Rev. B* **1996**, *54*, 13748−13758.
(8) Faupel, F.; Willecke, R.; Thran, A. *Mater. Sci. Eng., R* **1998**, *22*, 1−55.
(9) Strunskus, T.; Kiene, M.; Willecke, R.; Thran, A.; Bechtolsheim, C.; Faupel, F. *Mater. Corr* **1998**, *49*, 180−188.
(10) Song, W.; So, S.; Moulder, J.; Qiu, Y.; Zhu, Y.; Cao, L. *Surf. Interface Anal.* **2001**, *32*, 70−73.
(11) Song, W.; Li, Z.; So, S.; Qiu, Y.; Zhu, Y.; Cao, L. *Surf. Interface Anal.* **2001**, *32*, 102−105.
(12) Turak, A.; Grozea, D.; Feng, X.; Lu, Z.; Aziz, H.; Hor, A. *Appl. Phys. Lett.* **2002**, *81*, 766−768.
(13) Grandin, H.; Tadayyon, S.; Lennard, W.; Griffiths, K.; Coatsworth, L.; Norton, P.; Popovic, Z.; Aziz, H.; Hu, N. *Org. Electron.* **2003**, *4*, 9−14.
(14) Wang, X.; Xie, Z.; Wang, X.; Zhou, Y.; Zhang, W.; Ding, X.; Hou, X. *Appl. Surf. Sci.* **2007**, *253*, 3930−3932.
(15) Scharnberg, M.; Hu, J.; Kanzow, J.; Rätzke, K.; Adelung, R.; Faupel, F.; Pannemann, C.; Hilleringmann, U.; Meyer, S.; Pflaum, J. *Appl. Phys. Lett.* **2005**, *86*, 024104.
(16) Dürr, A.; Schreiber, F.; Kelsch, M.; Carstanjen, H.; Dosch, H.; Seeck, O. *J. Appl. Phys.* **2003**, *93*, 5201−5209.
(17) Gautier, E.; Lorin, A.; Nunzi, J.-M.; Schalchli, A.; Benattar, J.-J.; Vital, D. *Appl. Phys. Lett.* **1996**, *69*, 1071−1073.
(18) Neuhold, A.; Fladischer, S.; Mitsche, S.; Flesch, H.; Moser, A.; Novak, J.; Smilgies, D.; Kraker, E.; Lamprecht, B.; Haase, A.; Grogger, W.; Resel, R. *J. Appl: Phys.* **2011**, *110*, 114911.
(19) Langford, R. M.; Clinton, C. *Micron* **2004**, *35*, 607−611.
(20) Parratt, L. G. *Phys. Rev.* **1954**, *95*, 359−369.
(21) Dane, A. D.; Veldhuis, A.; De Boer, D. K. G.; Leenaers, A. J. G.; Buydens, L. M. C. *Phys. B: Condens. Matter* **1998**, *253*, 254−268.
(22) Croce, P.; Névot, L. *Rev. Phys. Appl. (Paris)* **1976**, *11*, 113−125.
(23) Li, H.; Bredas, J. L.; Lennartz, C. *J. Chem. Phys.* **2007**, *126*, 164704.
(24) Kiessig, H. *Annal. Phys.* **1931**, *10*, 769−788.